Electronic Supplementary Material (ESI) for Physical Chemistry Chemical Physics.

Iron and Oxygen Vacancies at the Hematite Surface: Pristine Case and Chlorine Adatom

Support Information

Raphael da Silva Alvim[1]*, Fabio Negreiros Ribeiro[2], and Gustavo Martini Dalpian[1]

[1]*Centro de Ciências Naturais e Humanas*
Universidade Federal do ABC
Santo André, SP, 09210-580, Brasil
[2]*Departamento de Química Teórica y Computacional*
Universidad Nacional de Córdoba
Córdoba, X5000HUA, Argentina

September 23, 2020

*raphael.alvim@ufabc.edu.br

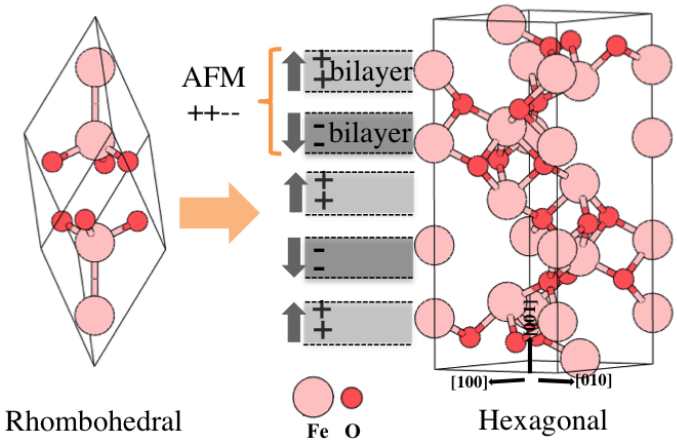

Figure-SI 1: Rhombohedral primitive and hexagonal conventional unit cells for the α-Fe_2O_3 bulk. Most stable antiferromagnetic (AFM) state and the magnetic state $++--$ in the Fe bilayers are showed. We firstly used the hematite bulk primitive cell with rhombohedral symmetry due to its decreased computational cost to obtain the best cut-off energies for the wave and electron density function, as well as the best k-point mesh for the convergence of the calculations. Accordingly, the wave functions and the electronic densities were respectively expanded employing cut-off energies of 0.54 keV and 2.72 keV with fine k-point mesh of $10\times10\times10$ in First Brillouin-Zone (FBZ).

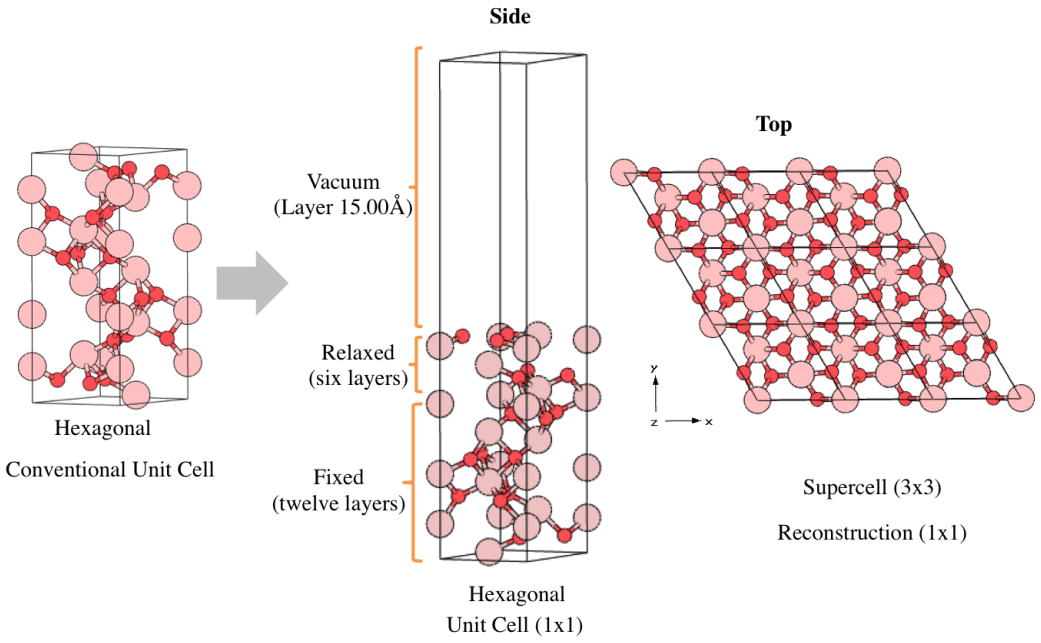

Figure-SI 2: Scheme for construction of the antiferromagnetic (AFM) hematite (001) surface from the hexagonal conventional unit cell. A supercell 3×3 was used due to the types of defects and adsorption to be studied: Fe and O vacancies, and Cl adatom adsorption. The wave functions and the electronic densities were respectively expanded employing cut-off energies of 0.54 keV and 2.72 keV with fine *k*-point mesh of $10\times10\times10$ in First Brillouin-Zone (FBZ) for the (001) surface with (1×1) cell, and Γ-point for (3×3) surface supercell with 270 atoms.

Table-SI 1: Gap energy (E_{gap}) and lattice parameters of the primitive rhombohedral (Rhom.) and conventional hexagonal (Hexa.) unit cells for the AFM hematite bulk resulting from different GGA+U functionals with spin-polarized. We tested the Perdew, Burke, and Ernzerhof (PBE)[a] and revised PBE (revPBE)[b,c] functionals to treat exchange-correlation interactions. The main difference between them is related to remotion of any van der Waals (vdW) parameter in revPBE. The errors related to gap and lattice parameters were obtained with respect to theoretical[d] (DFT+U) and experimental[e] (neutron diffraction) results in literature (Lit.), respectively. Energies, bond distances, angles and errors are in eV, Å, ° and %, respectively.

Hematite	Lit.	Bulk PBE+U			Bulk revPBE+U		
(α-Fe_2O_3)	Hexa.	Rhom.	Hexa.	Error	Rhom.	Hexa.	Error
Space Group				$R\bar{3}c$			
$\mathbf{E}_{gap}$	$\sim$2.00[d]	2.00	1.92	4.00	2.00	1.96	2.00
Lattice Parameters							
a	5.03[e]	5.52	5.12	1.79	5.56	5.16	2.58
b	5.03[e]	5.52	5.12	1.79	5.56	5.16	2.58
c	13.75[e]	5.52	13.98	1.69	5.56	14.08	2.40
α	90.00[e]	55.31	90.00	-	55.28	90.00	-
β	90.00[e]	55.31	90.00	-	55.28	90.00	-
γ	120.00[e]	55.31	120.00	-	55.28	120.00	-

[a]Perdew, J. P.; Burke, K.; Wang, Y. Generalized Gradient Approximation for the Exchange-Correlation Hole of a Many-Electron System. *Phys. Rev. B.* **1996**, *54*, 16533-16539.

[b]Perdew, J. P.; Burke, K.; Ernzerhof, M. Generalized Gradient Approximation Made Simple. *Phys. Rev. Lett.* **1996**, *77*, 3865-3868.

[c]Zhang, Y.; Yang, W. Comment on "Generalized Gradient Approximation Made Simple." *Phys. Rev. Lett.* **1998**, *80*, 890.

[d]Optical band-gap of 2.00-2.20 eV (Liao, P. et al. *Phys. Chem. Chem. Phys.* **2011**, *13*, 15189).

[e]Hill, A. H. et al. *Chem. Mat.* **2008**, *20*, 4891.

Table-SI 2: We tested the most important magnetic configurations of hematite through spin-polarized calculations according to structural energies. Energies in eV of the magnetic configurations $++--$, $+-+-$ and $+--+$ for the antiferromagnetic (AFM) state, as well as the respective $++++$ and zero magnetic state for ferromagnetic (FM) and nonmagnetic (NM), resulting from two different GGA+U functionals. The NM configuration was used as reference.

Magnetic state	**Configuration**	PBE+U	revPBE+U
	$++--$	-6.53	-7.32
AFM	$+-+-$	-5.92	-6.74
	$+--+$	-6.18	-6.99
FM	$++++$	-2.08	-2.74
NM	zero	0	0

Table-SI 3: Structural parameters of the Fe, FeO, α-Fe_2O_3 and Fe_3O_4 bulks, and the α-Fe_2O_3 1×1 surface calculated with PBE+U functional and spin-polarized. Bond distances and angles are in Å and °, respectively.

	Bulks				(001) Surface
	Fe	**FeO**	**α-Fe_2O_3**	**Fe_3O_4**	**α-Fe_2O_3**
Space Group	P1	C2/m	R$\bar{3}$c	Fd$\bar{3}$m	R$\bar{3}$c
Structural Parameters					
a	2.69	3.08	5.12	8.61	5.12
b	2.69	3.08	5.12	8.61	5.12
c	2.69	5.31	13.98	8.61	28.98
α	90.00	73.18	90.00	90.00	90.00
β	90.00	106.81	90.00	90.00	90.00
γ	90.00	120.14	120.00	90.00	120.00

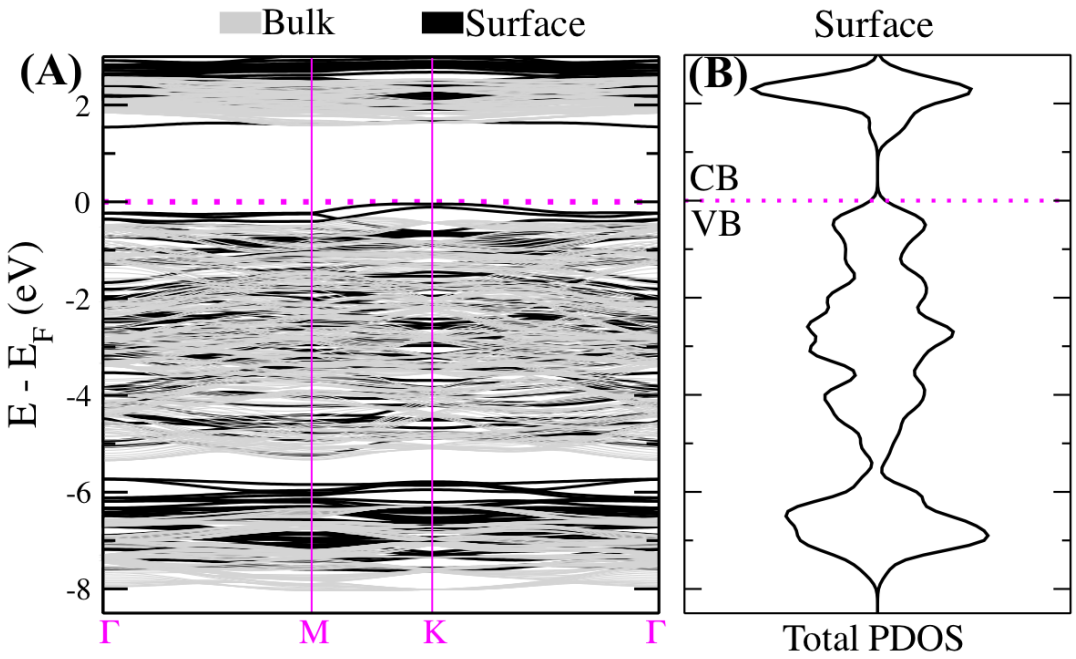

Figure-SI 3: In the case of the surface, it was necessary to calculate the band dispersion in order to compare the bands of the bulk with ones of the hexagonal surface. (A) Bands dispersion of hexagonal lattice displayed through the high symmetry points Γ-M-K-Γ for the antiferromagnetic (AFM) hematite structure. The bulk bands (gray lines) were projected on surface ones (black lines) with range from (k_x, k_y, 0.0) up to (k_x, k_y, 0.5) into variation of 0.1 in k_z. The structures of bands dispersion are referenced in the lowest core energy level in the bulk. (B) Projected density of states (PDOS) shows the contribution of the Fe-terminated hematite(001) surface in an 1×1 cell from the hematite bulk upon the conduction (CB) and valence (VB) bands. Therefore, the mid-gap states are a consequence of the surface.

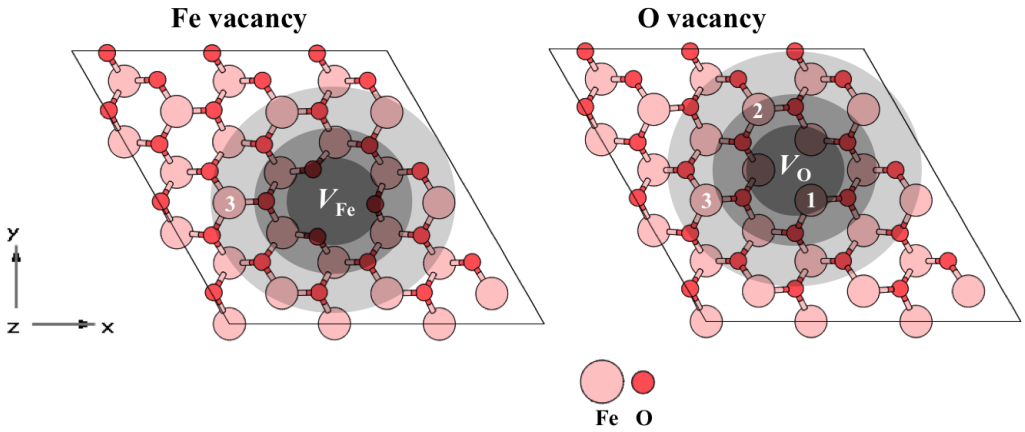

Figure-SI 4: In addition to the Fe (V_{Fe}) and O (V_O) vacancies, different types of top Fe nearest to V_{Fe} and V_O at the hexagonal supercell 3×3 for the hematite(001) surface are showed. We assumed three different radii with center in vacancy to figure out the three main top Fe sites (different shades of black are seen in the figure above). We choose the top iron sites 3 and 2 closest to V_{Fe} and V_O, respectively, since the remainder resemble the perfect hematite(001) surface. In particular at surface with V_O, the top iron site 2 was chosen because it is closest to vacancy and attending outside that.

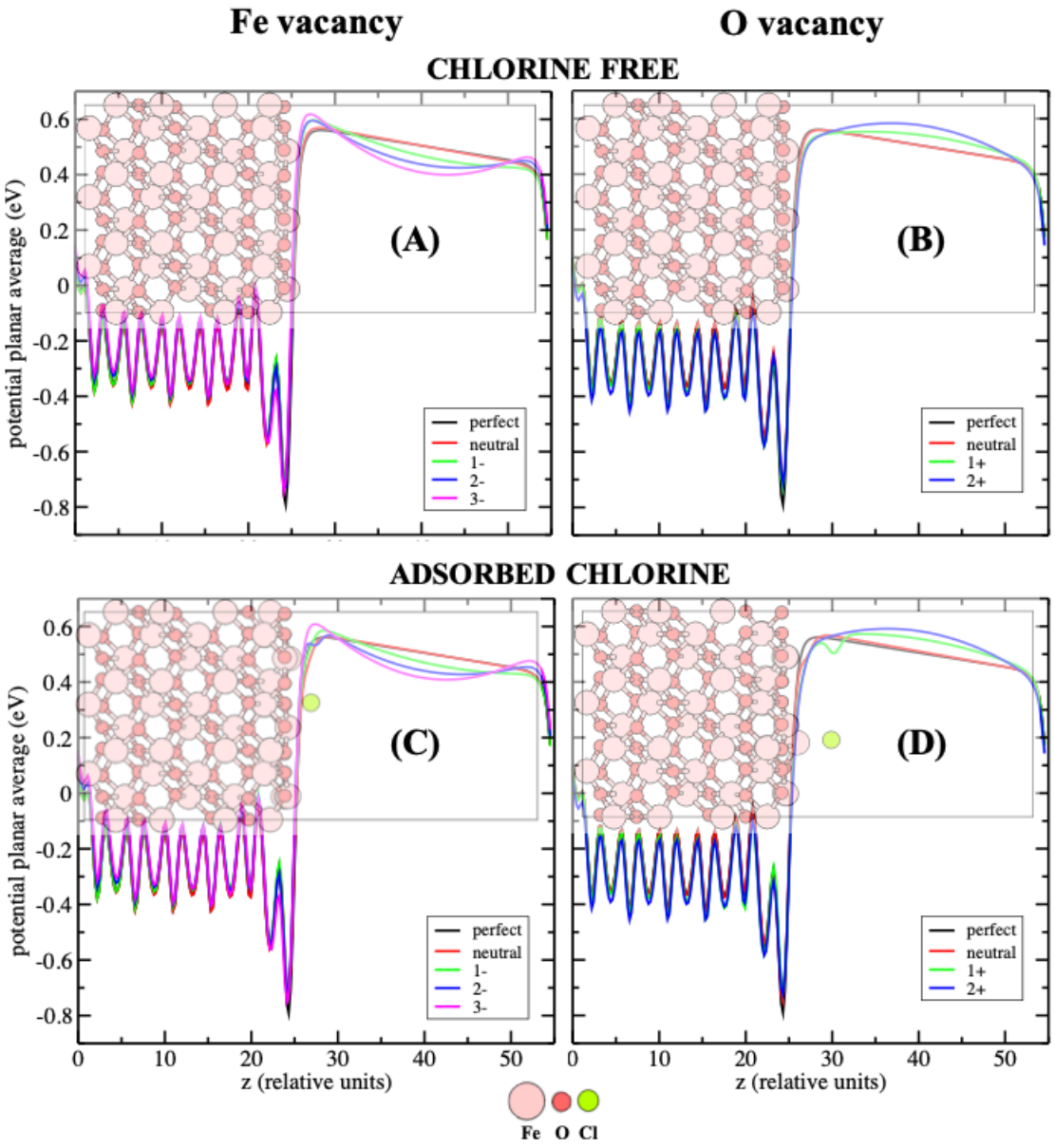

Figure-SI 5: Planar average of the total electrostatic potential energies (Hartree) for the perfect hematite(001) surface, with neutral and charged Fe (states 1-, 2- and 3-) and O (states 1+ and 2+) vacancies, with free and adsorbed Cl situations. (A) Fe vacancy, (B) O vacancy, (C) Fe vacancy and adsorbed Cl, and (D) O vacancy and adsorbed Cl. There is a slope of the potential in the vacuum region that is related to the electric field inside it, which arises after the surface cleavage of the Fe bilayer and consecutive separation of the Fe monolayers within a larger vacuum layer. The potential is decreasing and increasing at the vacuum layer region due to the additional and missing electrons at the surface vacancy, respectively. We used the average of the planar average in the middle of the hematite slab to ensure the non-influence of surface charge due to absence of potential correction in layer vacuum.

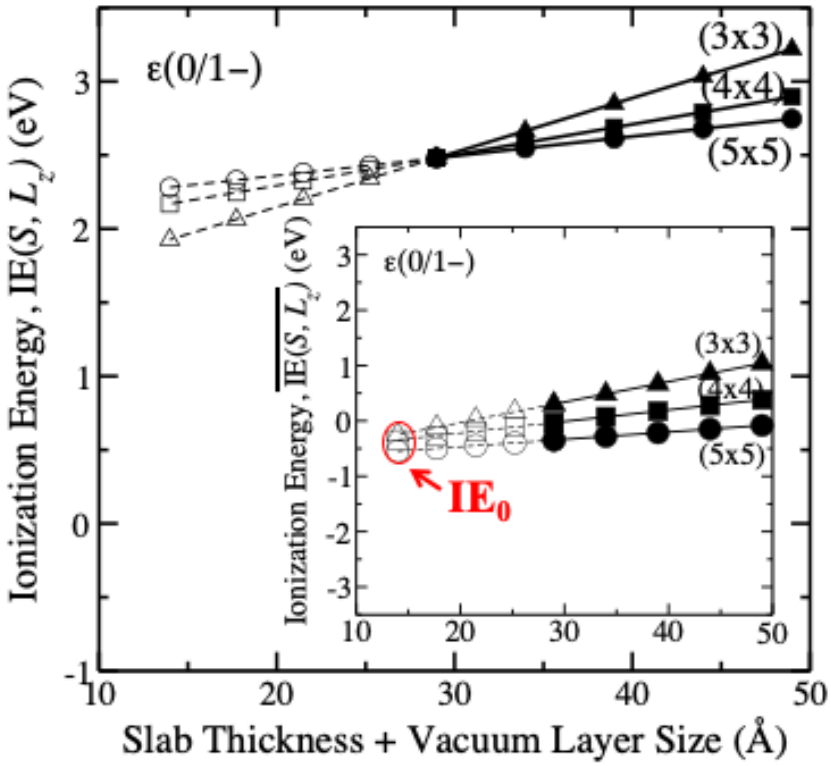

Figure-SI 6: We consider the continuous electrostatic problem of a charged plane in an uniformly compensating background ($L_z \gg L_x, L_y$) to neglect the terms related to S, since the large lateral dimensions have less contribution in the ionization energy and increase the computational cost. One can then use the appropriate physical limit at finite S and an interception at $L_z \to 0$. We then obtained the curves of ionization energy (IE) from Equation (2) in main text, thereby making the $\mathrm{IE}(S, L_z)$-intercept in 15.00 Å for the $\epsilon(0/1-)$ charge transition through different cell sizes (regression up to vacumm layer size $L_z = 0$): (3×3) (triangle), (4×4) (square) and (5×5) (circle) supercells with 270, 480 and 750 atoms, respectively. The vacuum layer size was ranged from 15.00 up to 35.00 Å with steps of 5.00 Å. Inset: to make it clear the size-independent ionization energy term (IE_0) through the common intercept of the lines regardless of S, we calculate the first degree polynomial $\overline{\mathrm{IE(S, L_z)}} = \mathrm{IE}(S, L_z) - \frac{\alpha}{\sqrt{S}} = \left(\frac{\beta}{S}\right) L_z^{'} + \mathrm{IE}_0$. The $\mathrm{IE}(S, L_z)$-intercept value is within a possible error marge of ± 0.10 eV due to same material Madelung constant and dielectric constant used in presence of the charged point defect (Wang, D. et al. *Phys. Rev. Lett.* **2015**, *114*, 196801). As the IE correction is indeed as larger as charge state increases in the vacant (3×3) supercell, it was used the IE_0 proportion from the $\epsilon(0/1-)$ correction to each vacancy charge transition $\epsilon(q/q^{'})$ in Equation (1) at main text.

Lee et al.[1] showed that the inclusion of the first term of monopole-monopole interaction resulting from the asymptotic result for the total electrostatic energy in the Makov-Payne (MP) scheme[2] has good convergence for the vacancy formation energy in the 3D hematite for the same supercell 3×3 with 270 atoms used here. The MP scheme is defined as follows:

$$E_{\mathrm{MP}} = \frac{q^2\alpha}{2\epsilon_{\mathrm{r}}L} + \frac{2\pi qQ}{3\epsilon_{\mathrm{r}}L^3} + \mathrm{O}(L^{-5}) \tag{1}$$

where α, ϵ_{r} and L for hematite are respectively the Madelung constant with experimental value of 67.34[3], the static (relative) dielectric constant with experimental value of 26.41[4], and the calculated cell-size parameter of $\sqrt[3]{V}$ = 18.08 Å. Q is the is the second radial moment of defect charge distribution. The last term in the righ side is the converged energy according to the asymptotic growth rate of L for neutral defects.

[1] Lee, J.; Han, S. Thermodynamics of Native Point Defects in α-Fe_2O_3: An ab initio Study. *Phys. Chem. Chem. Phys.* **2013**, *15*, 1890.

[2] Makov, G.; Payne, M. C. Periodic Boundary Conditions in *ab initio* Calculations. *Phys. Rev. B* **1995**, *51*, 4014-4022.

[3] Gool, W. V.; Piken, A. G. Lattice Self-Potentials and Madelung Constants for Some Compounds. *J. Mat. Sci.* **1969**, *4*, 95-104.

[4] Lunt, R. A.; Jackson, A. J.; Walsh A. Dielectric Response of Fe_2O_3 Crystals and Thin Films. *Chem. Phys. Lett.* **2013**, *586*, 67-69.

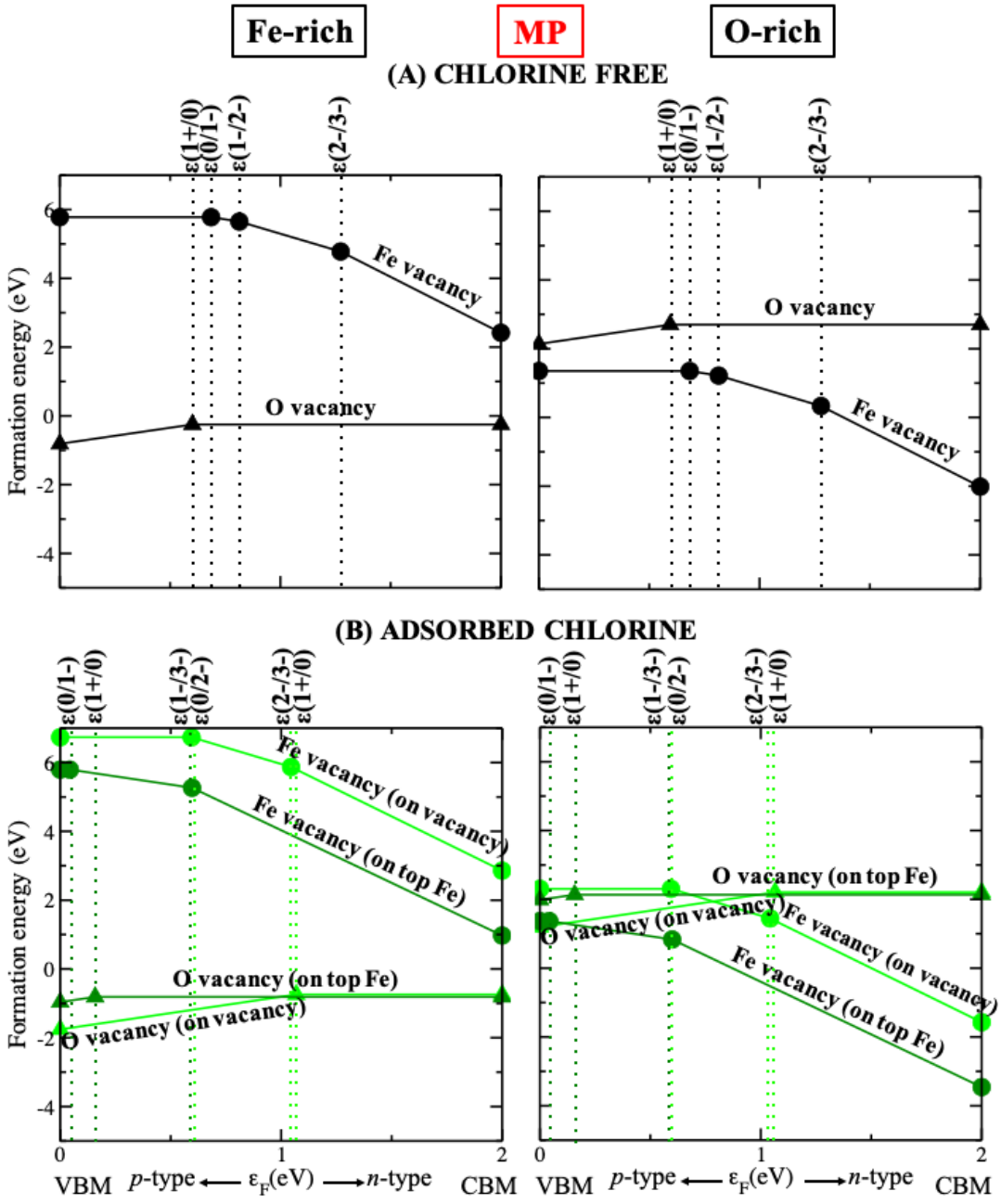

Figure-SI 7: The formation energy curves are showed according to Equation (1) in main text for the Makov-Payne (MP) correction related to the first monopole-monopole term in Equation (1) of the Support Information. (A) Chlorine free (black lines) and (B) adsorbed chlorine (green lines) are related to the Fe and O vacancies represented by circles and triangles, respectively. The neutral/charged Fe (V_{Fe}^{0}, V_{Fe}^{1-}, V_{Fe}^{2-} and V_{Fe}^{3-}) and O (V_{O}^{0}, V_{O}^{1+} and V_{O}^{2+}) vacancies were considered. In particular, the adsorption on the vacancy and top Fe sites are represented by light and dark green lines, respectively. The usual band-gap of 2.00 eV was used as the electronic potential range for the Fermi level between the valence-band maximum (VBM) and the conduction-band minimum (CBM) at each Fe-rich and O-rich thermodynamic limits.

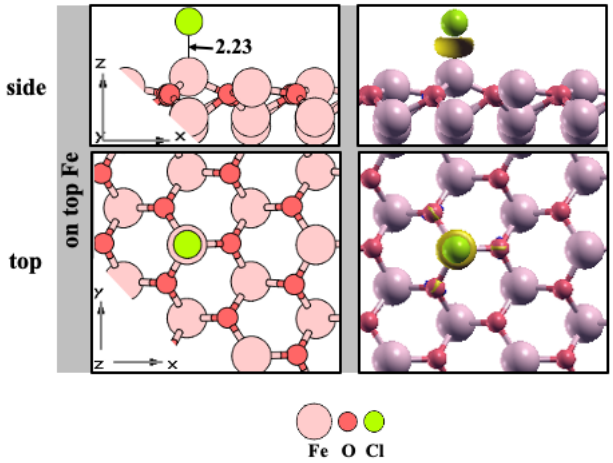

Figure-SI 8: (A) Adsorption of Cl on the top Fe sites at the perfect hematite(001) surface. Bond distances are in Å. (B) Charge density in the interface between Cl and the perfect hematite (001) surface. The yellow and blue colors indicate an increase and depletion in the charge density, respectively. The isosurfaces between ± 0.01 electrons$\times$Bohr^{-3} were used. Side and top views are showed.

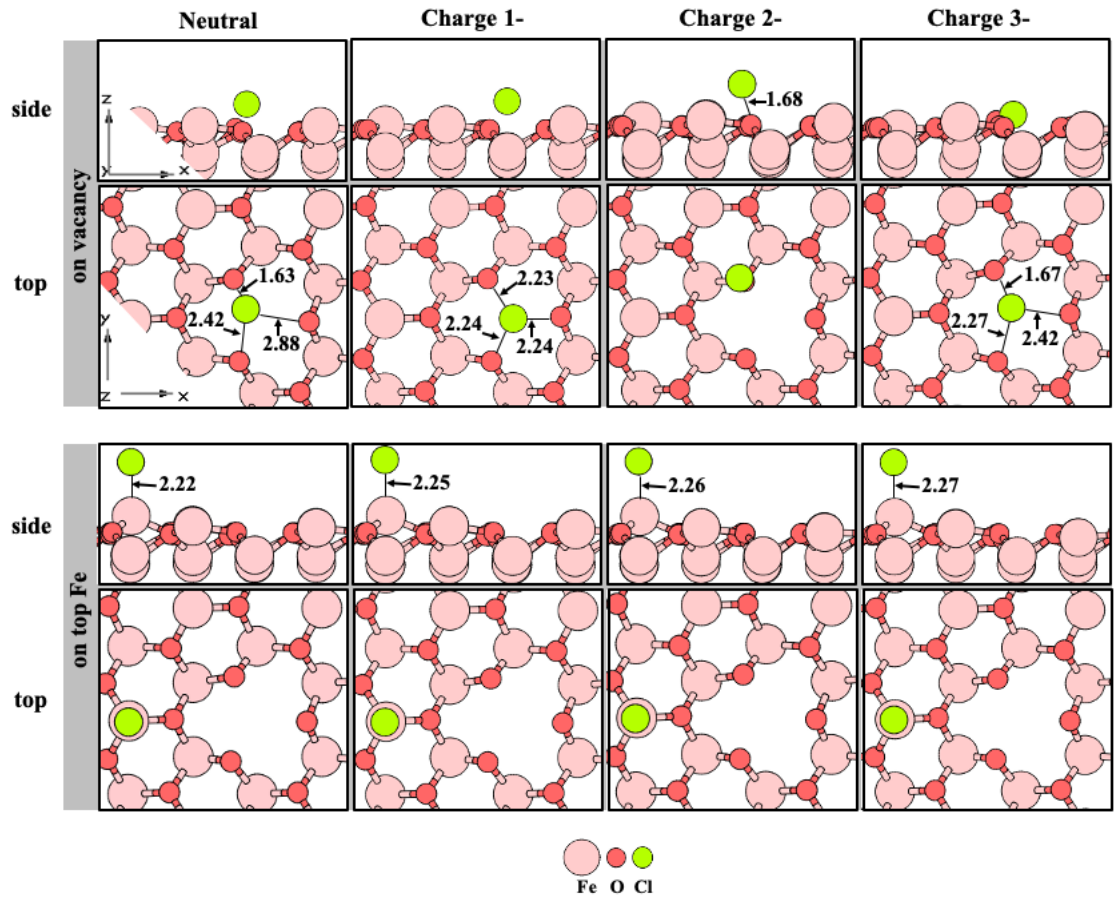

Figure-SI 9: Adsorption of Cl on the neutral Fe vacancy, and 1-, 2- and 3- charge states, and on their nearest top Fe at the perfect hematite(001) surface. Bond distances are in Å. Side and top views are showed.

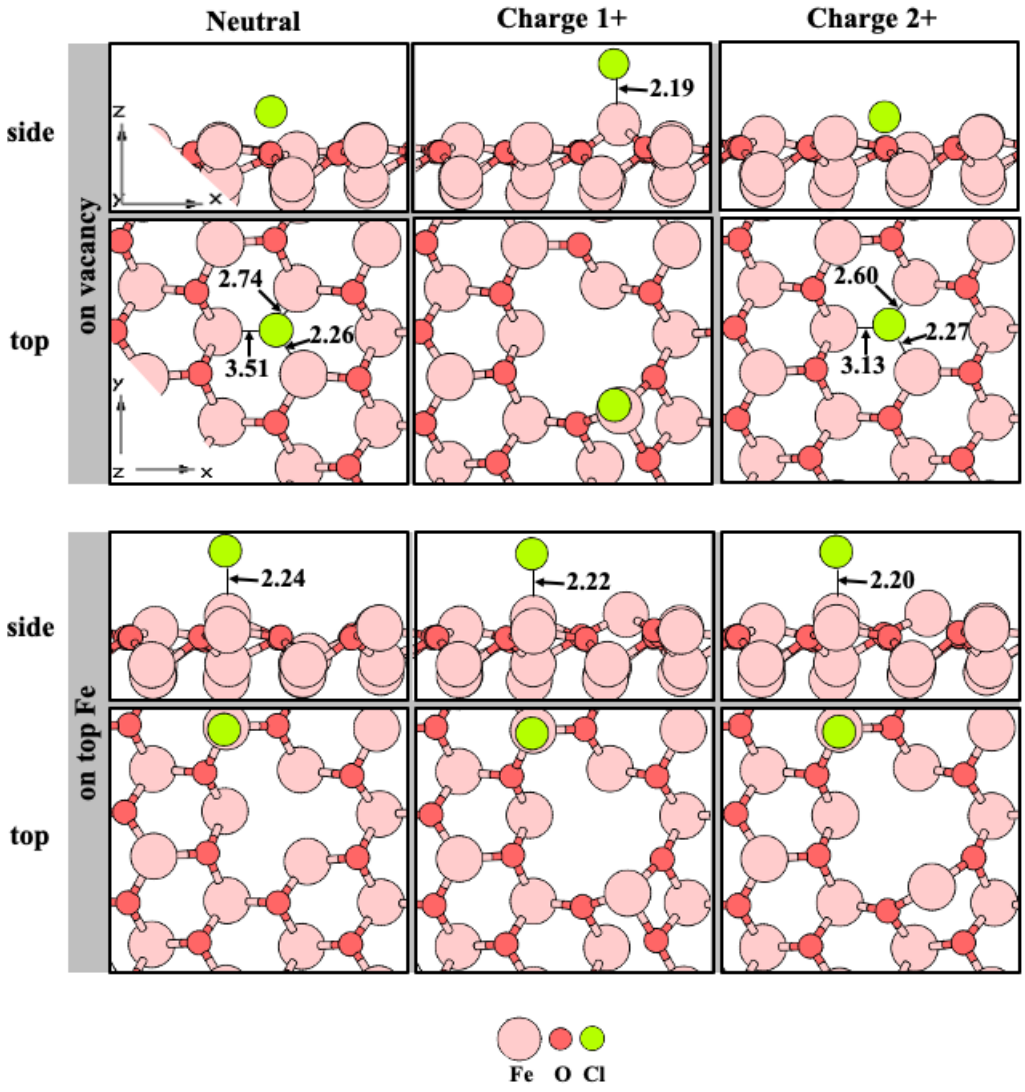

Figure-SI 10: Adsorption of Cl on the neutral O vacancy, and 1+ and 2+ charge states, and on their nearest top Fe at the perfect hematite (001) surface. Bond distances are in Å. Side and top views are showed.

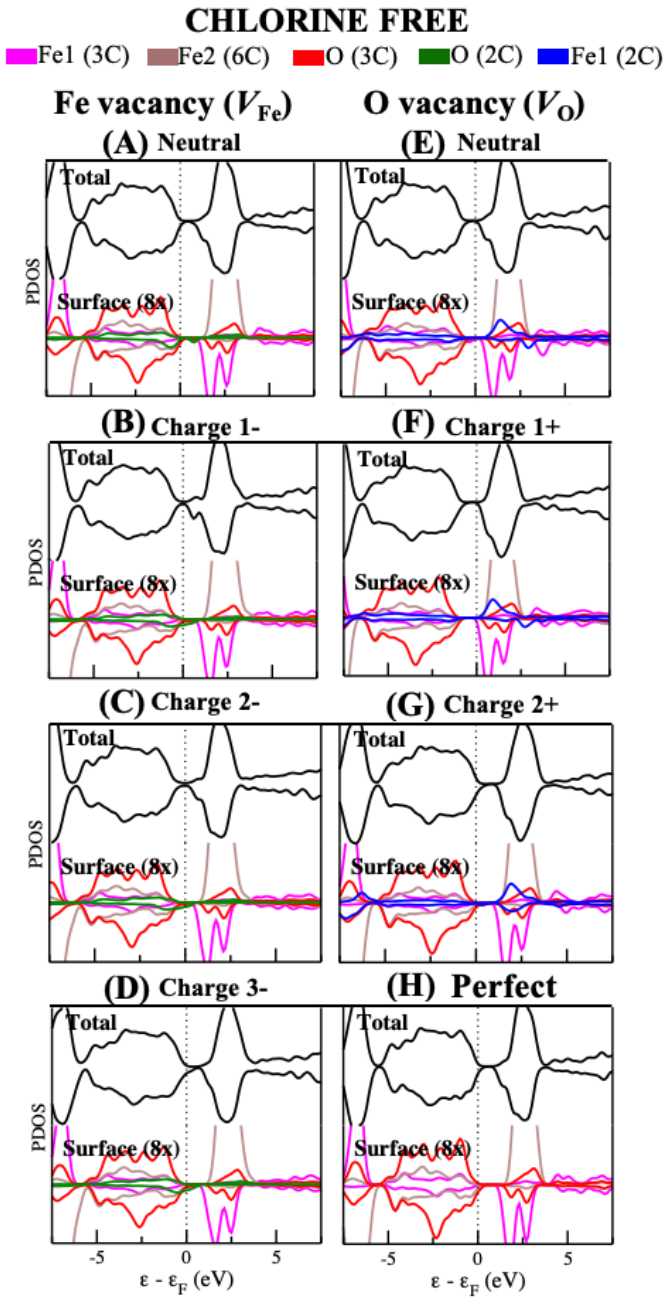

Figure-SI 11: Projected density of states (PDOS) for Cl free hematite(001) surface with: (A) the neutral Fe vacancy and with (B) 1-, (C) 2- and (D) 3- charge states, (E) the neutral O vacancy and with (F) 1+ and (G) 2+ charge states, and (H) the perfect sites. For the sites concerning to surface, we accounted the four optimized layers from top of the hematite(001) surface so that: Fe1 (3C) and Fe2 (6C) represent the three- (surface) and six- (bulk) coordinated Fe sites with up and down spin states, respectively, and O (3C) represents the three-coordinated O sites (surface); while O (2C) and Fe1 (2C) represent the two-coordinated sites of O and Fe due to the Fe and O vacancies, respectively.

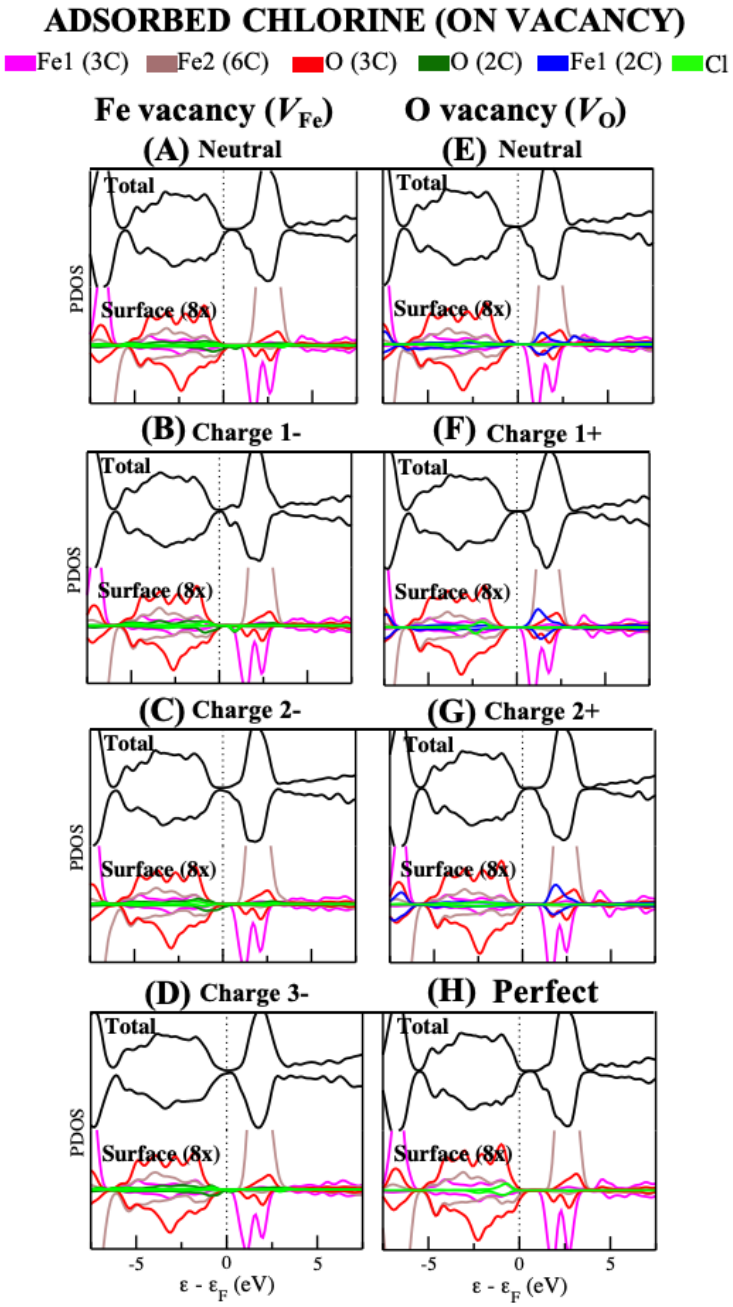

Figure-SI 12: Projected density of states (PDOS) for Cl adsorbed on: (A) the neutral Fe vacancy and with (B) 1-, (C) 2- and (D) 3- charge states, (E) the neutral O vacancy and with (F) 1+ and (G) 2+ charge states, and (H) the perfect hematite(001) surface. For the sites concerning to surface, we accounted the four optimized layers from top of the hematite(001) surface so that: Fe1 (3C) and Fe2 (6C) represent the three- (surface) and six- (bulk) coordinated Fe sites with up and down spin states, respectively, and O (3C) represents the three-coordinated O sites (surface); while O (2C) and Fe1 (2C) represent the two-coordinated sites of O and Fe due to the Fe and O vacancies, respectively.

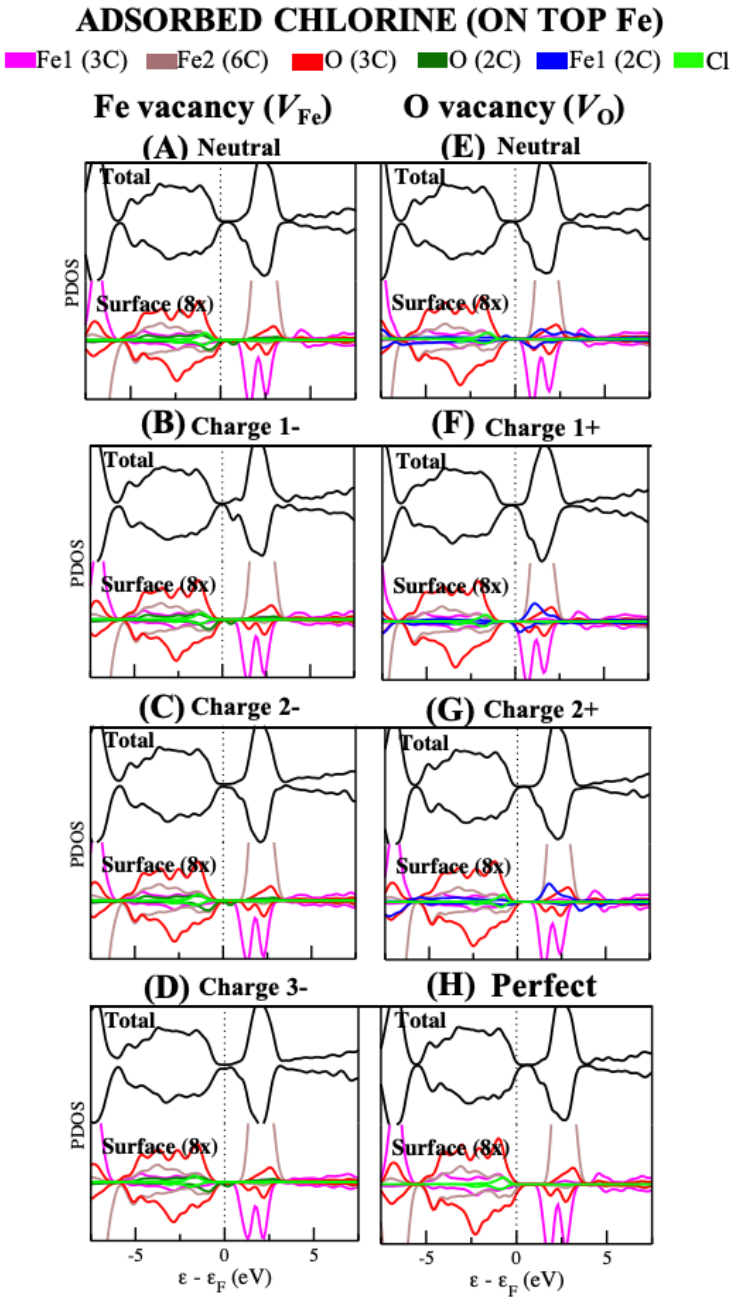

Figure-SI 13: Projected density of states (PDOS) for Cl adsorbed on the nearest top Fe with respect to: (A) the neutral Fe vacancy and with (B) 1-, (C) 2- and (D) 3- charge states, (E) the neutral O vacancy and with (F) 1+ and (G) 2+ charge states, and (H) the perfect hematite(001) surface. For the sites concerning to surface, we accounted the four optimized layers from top of the hematite(001) surface so that: Fe1 (3C) and Fe2 (6C) represent the three- (surface) and six- (bulk) coordinated Fe sites with up and down spin states, respectively, and O (3C) represents the three-coordinated O sites (surface); while O (2C) and Fe1 (2C) represent the two-coordinated sites of O and Fe due to the Fe and O vacancies, respectively.

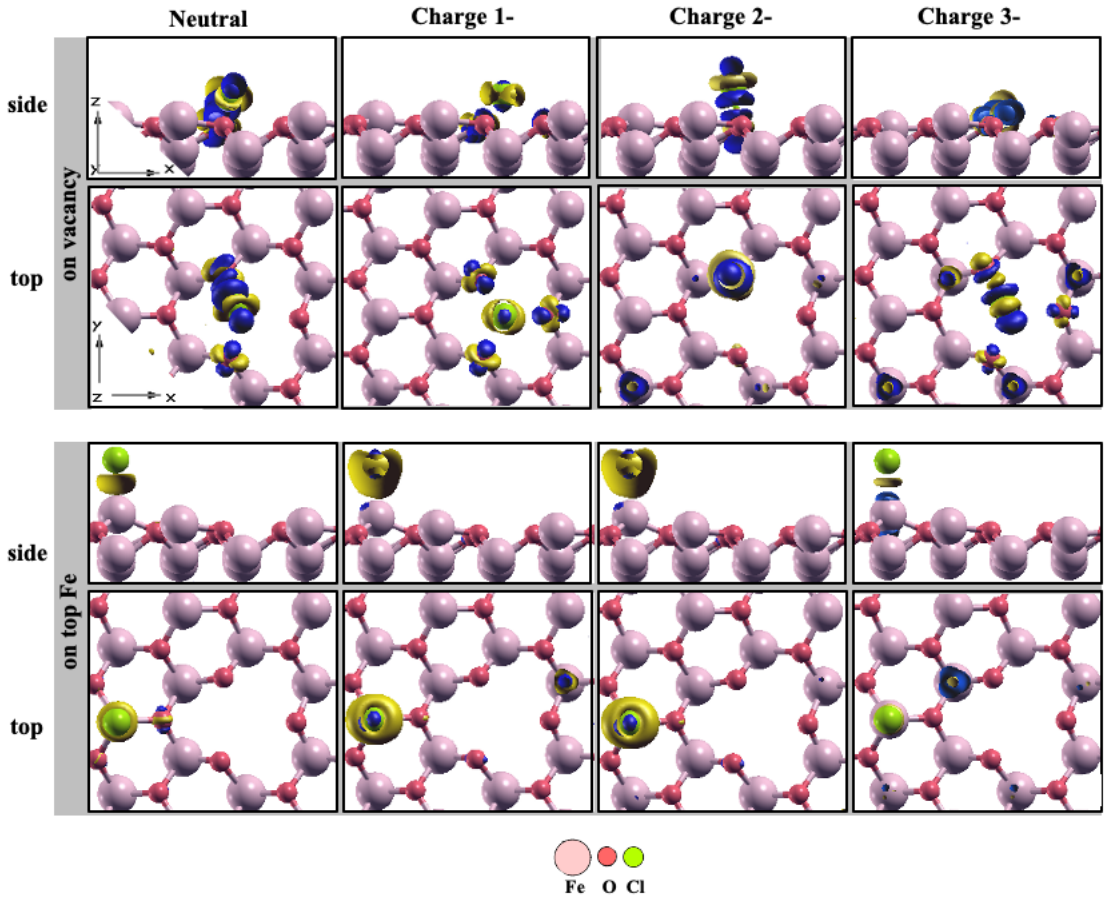

Figure-SI 14: Charge density calculated in the interface between the Cl adsorbed and the sites of vacancy and top Fe for the hematite(001) surface with neutral Fe vacancy and 1-, 2- and 3- charge states, and their nearest top Fe. The yellow and blue colors indicate an increase and depletion in the charge density, respectively. The isosurfaces between ± 0.01 electrons$\times$Bohr^{-3} were used. Side and top views are showed.

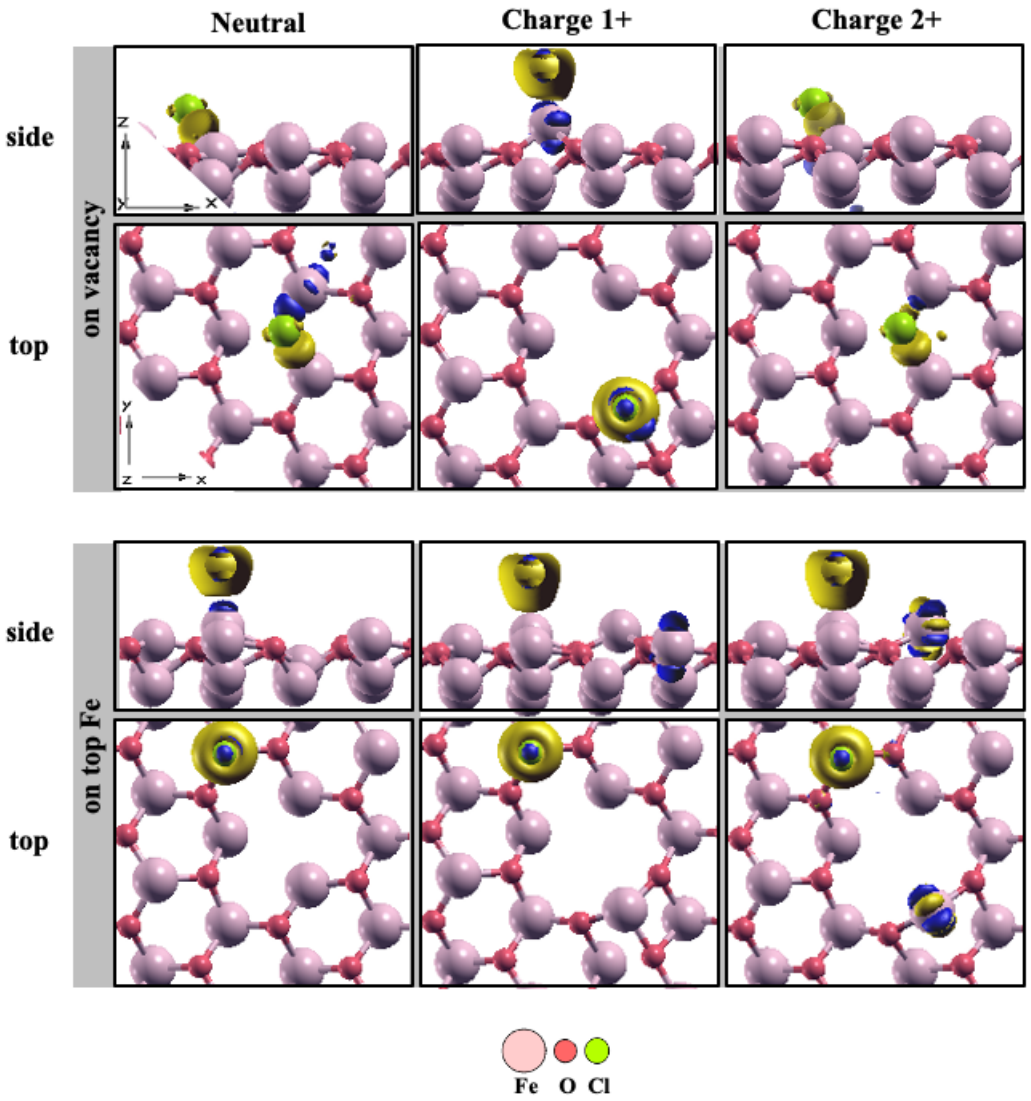

Figure-SI 15: Charge density calculated in the interface between the Cl adsorbed and the sites of vacancy and top Fe for the hematite(001) surface with neutral O vacancy and 1+ and 2+ charge states, and their nearest top Fe. The yellow and blue colors indicate an increase and depletion in the charge density, respectively. The isosurfaces between ± 0.01 electrons$\times$Bohr^{-3} were used. Side and top views are showed.